Proceeding of Coastal and Ocean Engineering in Korea (2002)
Vol. 13, pp. 191-197

Modeling buoyant surface discharges in a shallow channel with steady flow
정상 흐름하 천해역 수로에서의 저밀도수 표층방출 모델링

Kyung Tae Jung[1], Jae Youll Jin[1], Jin Soon Park[1], Ki Dai Yum[1],
Chang Wook Park[1], Sung Dae Kim[2], Suk Yoon[2]
정경태[1]·진재율[1]·박진순[1]·염기대[1]·박창욱[1]·김성대[2]·윤석[2]

1. INTRODUCTION

The prediction of the dynamic behaviors of buoyant water discharges into a large volume of water bodies, the flows of water accompanying the density differences due to temperature differences and sometimes also to salinity differences, have attracted great concern over several decades. Heated water surface discharges from power plants and freshwater discharges in estuaries are typical examples of the buoyant flows.

In this study, we present numerical experiments on the dispersion characteristics of surface discharges of low-density waters into a shallow channel in the presence of steady ambient flow. The problem considered was dealt with by many researchers in the course of developing turbulence models usually two- dimensional models (for example, McGuirk and Rodi, 1978; Choi et al, 1993). Three-dimensional structures are modeled here. Calculations are based on POM (Princeton Ocean Model) which employs a level 2.5 turbulence closure scheme (Mellor, 1998). The discharge source has been dealt with in a way similar to those used by Oey (1996) and Kourafalou et al (1996). A radiation condition originally developed by Flather (1976) has been adopted at the open boundaries in which the velocity has been basically assimilated and the associated surface elevation is defined by use of the geostrophic balance. Effects of changing the flow rate and/or the density of the water discharging into the channel are presented.

2. MODEL DESCRIPTION

2.1 The Model Domain

We consider a finite channel aligned parallel to x direction with a narrow discharge channel at the side of a lower wall. The dimension of the main channel is taken as 3.7km in width and 36km in length, while the dimension of the discharge channel is taken to be 70m in width and 540m in length. The open boundaries are located at the left and right ends of the main channel. Inflows are defined at the left open boundary and outflows are defined at the right open boundary. The discharge channel is 0.98km right of the inflow boundary and is aligned at right angle to the lower side wall.

The water depth h is assumed to vary only to the cross-channel direction (y direction), increasing linearly from the lower side wall to the upper side wall. In detail,

$$h(x, y) = 4 + 0.001(y - a) \tag{1}$$

where a is the y coordinate of the lower side wall. The water depth near the lower wall reaches a minimum of 4m, a maximum of 7.7m near the upper side wall.

Rectangular grids are constructed. Throughout the model domain the horizontal grid spacing is set to

[1] 한국해양연구원 연안·항만공학연구본부 (Coastal and Harbor Engineering Research Center, Korea Ocean Research and Development Institute, Ansan, Seoul 425-600, Korea)
[2] 한국해양연구원 해양데이터 운영팀 (Oceanographic Data Management Department, Korea Ocean Research and Development Institute, Ansan, Seoul 425-600, Korea)

100m to the cross-channel direction. The horizontal grid spacing to the direction parallel to the channel is fixed as 70m up to the point of x=6.3km, and is steadily increased by 10m, reaching a maximum size of 770m at the right open boundary.

2.2 The Governing Equations

We use in this study the time-dependent, three-dimensional, nonlinear, free surface, primitive equation model usually called POM (Princeton Ocean Model) in the literature (Mellor, 1998). In the model the incompressibility and hydrostatic balance are assumed along with Boussinesq approximation. The governing equations consist of continuity equation, momentum equations, transport equations of heat and salinity, two turbulence equations for turbulence energy and length scales, and the equation of state.

Finite-difference grids are used on the horizontal plane and the terrain-following coordinate is used in the vertical. The model uses a mode-splitting technique and the leap-frog scheme is used for time integration.

For the heat fields, the model solves the finite-difference analog of the following equation:

$$\frac{\partial DT}{\partial t}+\frac{\partial DUT}{\partial x}+\frac{\partial DVT}{\partial y}+\frac{\partial \omega T}{\partial \sigma} = \frac{\partial}{\partial \sigma}\left[\frac{K_v}{D}\frac{\partial T}{\partial \sigma}\right]+F_S \tag{2}$$

Here, T is water temperature, t is time, σ is the transformed vertical coordinate, U and V are the components of horizontal current, ω is the vertical component of velocity. K_v is the vertical eddy diffusivity coefficient, D is the instantaneous water depth, and F_S is the horizontal diffusion term.

The horizontal viscosity and diffusivity are parameterized by the Smagorinsky formula

$$K_H = c\Delta x\Delta y \mid \nabla \mathbf{U} + (\nabla \mathbf{U})^T \mid \tag{3}$$

where c is constant, which is taken as 0.2, ∇ is the horizontal gradient operator,, Δx and Δy are grid spacings, to x and y direction, respectively, and **U** is the velocity vector.

2.3 The Boundary Conditions

We specify downward vertical velocity at the head of the discharge channel which injects volumes and buoyant waters but no momentum. The continuity equation for the external mode is then modified as

$$\partial \eta / \partial t + \nabla \cdot D\underline{\mathbf{U}} = W_s \tag{4}$$

where W_S is the flow rate per unit area added to the top layer. Therefore, at the source point, (x_O, y_O),

$$W_s(x_O, y_O, t) = -Q/(\Delta x\Delta y), \tag{5}$$

otherwise W_S is set to zero. Along with the equation (4), the vertical velocity at the top of the source point is modified with addition of W_S.

The heat and salinity conservation equations are also modified with addition of $TW_s(2\Delta t_i)/D\Delta\sigma$, (here Δt_i is an internal mode time step) in the calculation of net horizontal flux.

The boundary conditions at the sea surface and bottom are:

$$\rho K_v\left(\frac{\partial T}{\partial \sigma}\right) = KD(T - Ta) \tag{6}$$

$$\rho K_v\left(\frac{\partial S}{\partial \sigma}\right) = 0, \tag{7}$$

where K_v is the heat loss coefficient, Ta is the ambient temperature, and S is the salinity. At the sea bottom the normal fluxes are set to zero.

For the flow no wind stress condition is taken at the sea surface and a quadratic friction law is applied at the sea bottom. For details, see Mellor (1998).

Now we describe the specification of open boundary conditions. The radiation condition originally developled by Flather (1976) for the two-dimensional tidal model is adopted.

$$\underline{U} - \underline{U}_O = \pm(Cg/h)(\eta - \eta_O) \tag{8}$$

where Cg is the speed of long gravity wave, $\underline{U}_o$ and η_O are the assimilated depth-averaged velocity and elevation, respectively, the relation of which is given by the geostrophic balance condition:

$$\eta_O = (f/g)\underline{U}_O \tag{9}$$

where g is the gravitational constant, f is the Coriolis factor chosen as 0.0001. In equation (8) "+" sign is chosen at the right side open boundary, "-" sign is chosen at the left side open boundary. Along with equation (9), the mean water level is

adjusted in a way such that the sea surface elevation goes to zero approximately at the middle of the channel.

3. EXPERIMENTS AND RESULTS

A series of model experiments are described below. All calculations have started from the initial state of no motion with uniform temperature and salinity fields (26°C and 33.5psu). The model runs have continued over 15 days. The time step for the external mode has been chosen as 2.4 seconds, the internal mode time step is chosen 3 times larger. The advection term has been also calculated every 3 external mode time steps. The convection terms are calculated using the first-order upstream plus Smolarkwicz iterative upstream scheme with an antidiffusion velocity (Smolarkiewicz, 1984). The assimilated velocity $\underline{U}_o$ is taken 0.5m/s .The heat loss coefficient is chosen as 32 w/m^2. A total of 11 layers are used in the vertical with a logarithmic variation, allocating finer levels near the sea surface and bottom.

Model results displayed below are shown over the channel area of 5.6km by 2.7km.

3.1 Heated Water Discharge

Initially, calculations of heated water are performed with temperature rise (ΔT) of 8°C, and the discharge flow rate Q=218.4 m^3/s, which are typical values in case 4 units of nuclear power plants are in operation.

Fig.1 shows the excess temperature distributions at the surface and near-bottom layers, superimposed on the velocity vectors drawn at every 3 grid intervals to the x direction. It is evident that shore attached plumes are formed due to the presence of strong cross-flow. No recirculation zone is therefore formed. It is noted that the heated water experiences strong initial mixing and thereby the excess temperature decreases rapidly in the near-field region, giving the very steep change in the excess temperature near the mouth of the discharge channel.

Outside of the initial mixing zone the isothermal contours are formed almost parallel to the ambient flow. High excess temperature contours appear on the side of lower side wall where the water depth is shallow. It is seen that the decay rate of the excess temperature in the far field region is very slow. Such behavior is indicated by CORMIX system (Jung et al, 2002) and an analytical solution. The far-field temperature rise in a channel of uniform depth due to a point source with intensity q may be given by

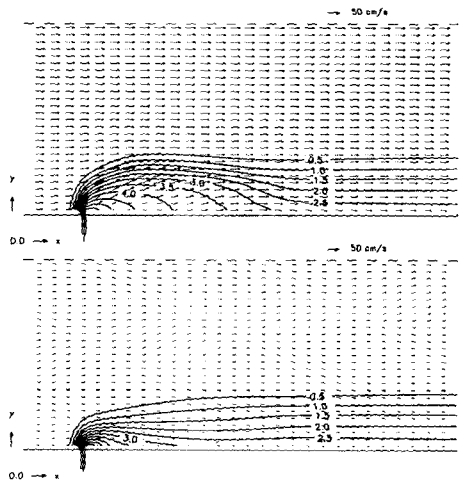

Fig .1. The excess temperature distributions at the surface and near-bottom layers computed with ΔT= 8°C, and Q=218.4 m^3/s.

$$T = \frac{q}{\pi h K_H} \exp(2\underline{U}_o x / K_H) Ko(Z)$$

$$+ \frac{q}{\pi h K_H} \exp(2\underline{U}_o x / K_H) Ko(Z') \qquad (10)$$

where Ko is the modified Bessel function of 2 nd kind (Abramowitz and Stegun, 1970) and

$$Z = (x^2 + y^2)^{1/2} (\underline{U}_o / 4K_H + K / K_H)^{1/2} \qquad (11)$$

$$Z = (x^2 + (y+b)^2)^{1/2} (\underline{U}_o / 4K_H + K / K_H)^{1/2} \qquad (12)$$

The 2 nd term in equation (10) is the contribution of an imaginary source located at the upper side wall. We can see from equation (10) that the excess temperature rise decays exponentially as the distance increases. For the prediction of near field temperature rise a line source model might be better suited rather than point source model. For the detailed derivation of point and line source solutions in an unbounded sea , see Atkins and Diver(1975).

The vertical structure is marginally noticeable even in the near field. That is, the temperature rise at the near-bottom layer is more or less similar to that of the surface layer. This is because the background mixing induced by cross-flow overwhelms the buoyancy force. As goes far downstream, a well-mixed structure appears.

Regarding the flow fields, it is interesting to note that, at the downstream region of the near field, the flows at the sea surface tend to goes away from the lower side wall, while the flows near the bottom direct tend to go to the side of lower wall. Outside the near-field region the directions of flow vectors are almost identical.

The velocities at the near-bottom are smaller than those of the sea surface due to bottom friction. At the very near to the lower side wall the flow intensity is weaker than other parts..

Fig.2 displays the temperature rise at the sea surface computed with Q=112.8 m^3/s , and Q=354.6 m^3/s , fixing ΔT as 8°C, keeping in mind 2 and 6 units operation. The calculated discharge velocities at the mouth of the discharge channel are 0.55m/s and 1.26m/s, respectively (in case of Q=218.4 m^3/s , the velocity at the mouth of the discharge channel is 0.98m/s). Therefore, in the 1st case the densimetric Froude number defined by (Miller and Brighouse, 1984)

$$Fo = U_d (\Delta\rho / \rho g h)^{-1/2} \qquad (13)$$

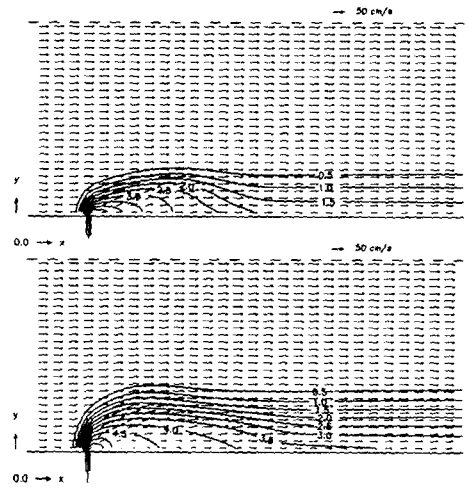

Fig. 2. The excess temperature distributions at the surface layer computed with Q=112.8 m^3/s (upper), and Q=354.6 m^3/s (lower), fixing in both cases ΔT as 8°C.

is about 43% smaller than that of 4 unit case, while in the 2 nd case the densimetric Froude number is 29% larger than that of 4 unit case. In equation (13) U_o is the discharge velocity, and $\Delta\rho$ is the density difference between the discharge water and the ambient water. The densimetric Froude number represents the ratio of inertial force to buoyancy force.

Again shore attached plumes are formed but in different width according to the amount of the discharged heat. As the discharge flow rate is increased, the buoyant flow penetrates to the deeper region, interacting more with the cross-flow and forming a thermal plume of wider band. Reverse effects are noted when the discharge rate is reduced. The maximum reaches of isotherms to the x-direction are not proportional to the discharge rate. The width of the far-field plume when the flow rate is increased is 30% increased than the case computed with Q=112.8 m^3/s . Higher excess temperature rise occurs when the flow rate is increased.

Fig.3 displays the distributions of temperature rise from two experiments, one with Q=145.6 m^3/s and ΔT as 12°C, another with Q=327.6 m^3/s and ΔT as 5.3°C, fixing in both cases the total heat discharge rate. The densimetric Froude number of the former experiment is significantly smaller than that of the 2nd. Again shore attached plumes are formed but in different form. When the densimetric Froude number is small, the buoyant structure is pronounced, showing the patterns with steep isothermal contours in the near-field region. As the Froude number is increased, the buoyant flow becomes less pronounced, showing a smooth variation in the near-field region. As goes to the far-field region, the patterns are reversed; the width of the thermal plume becomes narrower and the gradient of isothermal contours becomes steeper in high densimetric Froude number case, comparing with the results computed for the low densimetric Froude number. In both cases the excess temperature rises decay slowly.

It is interesting to note that there is a hint of recirculation zone tends to form at the right of the discharge channel.

3.2 Low Salinity Water Discharge

Fig.4 shows the salinity distribution (S-Sa) at the surface and near-bottom layers computed with S=17.5psu, and Q=218.4 m^3/s. It is seen that the vertical mixing is very much suppressed, comparing with heated water discharge considered in this study.

In the near-field region the main axis of the plume is slightly shore-detached and at the further

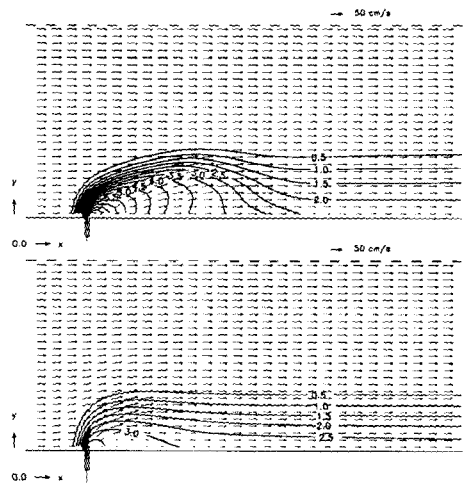

Fig. 3. The excess temperature distributions computed with Q = 145.6 m^3/s and ΔT = 12°C (upper), and Q = 327.6 m^3/s and ΔT =5.3°C (lower).

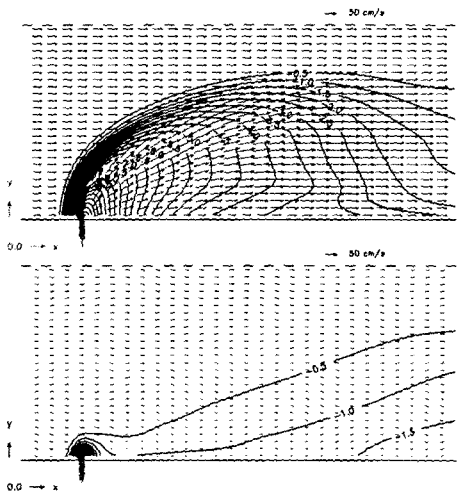

Fig. 4. The distribution of low salinity water at the surface and near-bottom layers computed with S=17.5psu, and Q=218.4 m^3/s.

downstream a shore-attached plume tends to form. It is interesting to note that the at the sea bottom the salinity distribution is very different; the contour lines meet with the lower side wall at a slant angle and higher concentration appear at the downstream side rather than near the mouth of the discharge channel.

The tendency shown in the heated water discharge again appears in the velocity fields. That is, at the downstream region of the near field, the flows at the sea surface tend to goes away from the lower side wall, while the flows near the bottom direct tend to go to the side of lower wall.

Fig.5 shows the salinity distribution (S-Sa) at the surface layer computed with S=25.5psu and 0 psu, fixing Q=218.4 m^3/s. Calculation with 0 psu corresponds to the discharge of pure freshwater. Shore-detached plumes are formed in both cases. In case of calculation with 0 psu at the source the buoyant flow dominates over the channel. Even with 25.5psu the buoyant flow is more prominent comparing with the case of the heated water. However, a sign of developing recirculation zone is absent.

4. CONCLUSION

In order to examine the dynamic behaviors of buoyant surface discharges, a series of numerical experiments has been made using POM in an idealized finite channel with steady cross-flow. The basic code has been modified to accommodate not only the surface discharge of low-density water but the heat loss, which is linearly proportional to the temperature rise. Further extension of the model is possible. For example, the sea surface slope can be added in case an intrinsic slope exists along the discharge channel.

Experiments have been in this study designed to examine the behaviors of the discharged waters having different values of the densimetric Froude number. It has been seen that the dominance of the inertial force forces the discharge water allows the buoyant flow to penetrate farther to the interior of the channel and thereby a plume of wider band is formed to the downstream direction. The dominance of buoyancy force tends to cause strong lateral spreading as well as surface trapping of the discharge waters.

The model results are qualitatively in good agreements with the results obtained from CORMIX3; shore attached plumes are developed and very slow decay is shown as goes to far-field region. It is expected that the slow decay at the far-field might inhibit correct estimates of the thermal spreading distance through field observations.

Further studies will be followed by taking into account wind effects and tidal forcing. One of our immediate concern is to investigate the thermal spreading in the presence of jetties at the offshore of the discharge channel.

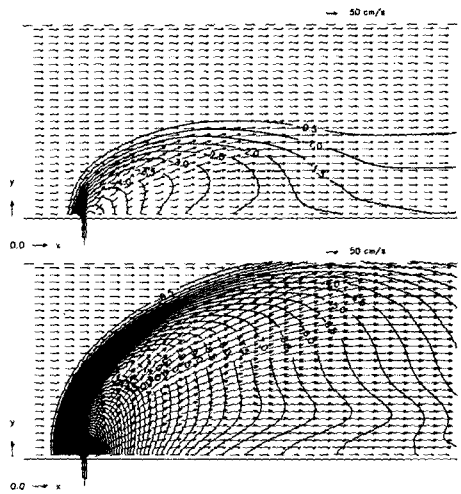

Fig. 5. The distribution low-salinity water at the surface layer computed with S=25.5psu and 0 psu, fixing and $Q = 218.4\ m^3/s$.

ACKNOWLEDGMENTS

This research has been funded by Ministry of Environment through the project " A GIS based study of developing monitoring techniques of coastal environmental change" and by Ministry of Scinece and Technology through the project " A study on the transport process of contaminants in the Yellow Sea".

REFERENCES

Abramowitz, M. and Stegun, I.A., 1970. Handbook of mathematical functions, Dover Publications, Inc., p.1046.

Atkins, R., and Diver, C.F.M, 1975. Mathematical modelling of heated discharges in tidal flow 2. Plume development and dispersion, Hydraulics Research station, Report no. INT 147.

Choi, H.S., Jung, K.T., So, J,K. and Lee, K.S., 1993. A two-dimensional turbulence model for the thermal discharge into crossflow. field, *J. Korean Soc. Coastal Ocean Engr.*, 5(2), pp.91-98.

Flather, R.A, 1976. A tidal model of the northwest. European Continental Shelf, *Mem. Soc. Roy. Sci. Liege*, 10, pp.141-164

Jung, K.T., kim, S.D., Park, C.W., Jin, J.Y., J.S. and Park, So, J,K., 2002. Far-field prediction of the dispersion of thermal effluents in a shallow coastal sea region using the CORMIX system, *Proc. KOSMEE Spring Annual meeting,* , held at Cheju, May 10, pp.257-263.

Kourafalou, V.H., Lee, T.N., Oey, L.-Y., and Wang, J.D., 1996. The fate of river discharge on the continental shelf 2.Transport of coastal low-salinity waters under realistic wind and tidal forcing, *J.Geophys. Res.*,101(C2), pp.3435-3455.

McGuirk, J.J. and Rodi, W., 1978. A depth-averaged mathematical model for the near-field of side discharge into open-channel flow, *J. Fluid Mech.*, 86(4), pp.761-781.

Mellor, G.L., 1988. Users guide for a three-dimensional primitive equation, num erical ocean model, p.41.

Miller, D.S. and Brighouse, B.A., 1984. Thermal discharges, British Hydromech. Res. Asso., p.221.

Oey, L.-Y., 1996. Simulation of mesoscale variability in the Gulf of mexico: sensitivity studies, comparison with observations, and trapped wave propagation. *J. Phys. Oceaogr.*, 26, pp.145-175.

Smolarkiewicz, P.K., 1984. A fully multi-dimensional positive definite advection transport alogorithm with small implicit diffusion, *J. Compu. Phys.*, 54, pp.325-362.